Scientia Iranica C (2023) 30(6), 2043–2055

Sharif University of Technology
**Scientia Iranica**
*Transactions C: Chemistry and Chemical Engineering*
http://scientiairanica.sharif.edu

# Alumina-PEBA/PSf Multilayer composite membranes for $CO_2$ separation: Experimental and molecular simulation studies

**M. Elyasi Kojabad[a,b], M. Nouri[a,b], A.A. Babaluo[a,b,*], A. Tavakoli[a,b], R. Sardari[a,b], Z. Farhadi[a,b], and M. Moharrami[a,b]**

a. *Faculty of Chemical Engineering, Sahand University of Technology, Tabriz, Iran.*
b. *Nanostructured Materials Research Center, Sahand University of Technology, Tabriz, Iran.*

Received 10 February 2021; received in revised form 25 July 2022; accepted 26 December 2022

**KEYWORDS**
PEBA;
Multilayer mixed matrix membranes;
$\alpha$-$Al_2O_3$ particles;
$CO_2$ separation;
Molecular simulation.

**Abstract.** In this research, Polyether Block Amide (PEBA) containing different loadings of $\alpha$-$Al_2O_3$ particles was deposited on top of the polysulfone (PSf) supports to form PEBA 1657-$\alpha$-$Al_2O_3$/PSf Multilayer Composite Mixed Matrix Membranes (MCMMMs). Multilayer composite structure was employed to overcome the sedimentation of fillers in the polymer matrix. Moreover, alpha phase of $Al_2O_3$ particles was applied to improve the distribution of these particles at higher loadings. Scanning Electron Microscopy (SEM), X-Ray Diffraction (XRD), and Fourier Transforms Infrared spectroscopy (FTIR) tests were applied to study morphology, crystalline structure, and chemical structure of the membranes, respectively. Gas permeation properties of the membranes were also measured using three different pure gases ($CO_2$, $CH_4$, and $N_2$) at a pressure of 7 bar and temperature of 25°C. $CO_2$ permeance and ideal selectivity of $CO_2/CH_4$ and $CO_2/N_2$ for the optimum MCMMM with 20 wt.% loading of $\alpha$-$Al_2O_3$ particles were 25% (117.5 Barrer), 81.5% (32), and 86.5% (57) higher than those of Multilayer Composite Neat Membrane (MCNM), respectively. The molecular simulation results confirmed the results of the experimental studies and approved that the $\alpha$-$Al_2O_3$ particles were the right candidates to improve the PEBA performance for $CO_2$ separation.



## 1. Introduction

Over the past few decades, concerns about greenhouse gas emissions have increased rapidly. The emission of greenhouse gases is the major cause of global warming. Carbon dioxide is known as a greenhouse gas that is causing climate change [1–5]. Recently, membrane separation as a state-of-the-art technology can facilitate separating the carbon dioxide from the flue gases of the combustion processes and it has many advantages such as low energy consumption, small footprint, environmentally friendliness, and ease of scale-up [6,7]. Among different types of $CO_2$ separation membranes, polymeric membranes play an important role because of their ease of fabrication, low cost, and superior modularity [8,9].

In recent decades, various polymers such as polysulfone, polyimide, polyphosphazene, cellulose acetate, polyurethane, and Polyether Block Amide (PEBA) copolymer have been used as membrane materials for $CO_2$ separation [10]. Among these polymers, PEBA is the most interesting material and is the right candidate

*. *Corresponding author. Tel.: +984133458085; Fax: +984133458084*
*E-mail address: a.babaluo@sut.ac.ir (A.A. Babaluo)*

doi: 10.24200/sci.2022.57717.5383

for $CO_2$ separation from flue gas and natural gas due to its high selectivity coefficients (e.g., $CO_2/N_2$ or $CO_2/CH_4$) [11–13].

However, PEBA polymeric membranes are mainly used for $CO_2$ separation; these membranes cannot overcome the trade-off limitation between permeability and selectivity. Therefore, several methods have been developed to overcome this limitation in PEBA polymeric membranes [14–24].

Among different relevant methodologies, incorporating metal oxide particles (such as $SiO_2$, $TiO_2$, and $Al_2O_3$) into polymeric membranes to produce mixed matrix membranes has been extensively studied in recent years [14,15,17,18]. These particles can increase $CO_2$ solubility through the membranes because of their intrinsic affinity to $CO_2$ in comparison with $N_2$ and $CH_4$, leading to high selectivity of $CO_2/N_2$ and $CO_2/CH_4$; however, the kinetic diameter of $CO_2$ (3.3 Å) is smaller than that of $N_2$ (3.64 Å) and $CH_4$ (3.8 Å). Moreover, the availability and low prices of these particles make them a suitable choice for the preparation of mixed matrix membranes in the case of $CO_2/N_2$ and $CO_2/CH_4$ separations [19–22]. Some researchers have studied the incorporation of metal oxide particles such as $TiO_2$ [11,24], ZnO [25,26], $SiO_2$ [27,28], and $\gamma$-$Al_2O_3$ [29] into PEBA membranes, which improved the separation performance of this polymer. Azizi et al. fabricated a mixed matrix membrane by dispersing $SiO_2$, $TiO_2$, and $\gamma$-$Al_2O_3$ into PEBA 1074 and compared the permeability performance of these three types of mixed matrix membranes. The results indicated that by embedding $\gamma$-$Al_2O_3$ nanoparticles, the membrane exhibited a considerable ability to pass $CO_2$ molecules in comparison with the two other membranes because enhanced $CO_2$ permeability and $CO_2/CH_4$ selectivity were 48% and 28%, respectively, compared to PEBA membrane [22]. However, the mentioned works offered mixed matrix membranes with improved separation performances in comparison with neat PEBA; they could not increase particle loadings to high contents due to agglomeration of metal oxide particles and migration to the surface or sedimentation of these particles. The migration to the surface and/or sedimentation of particles can be efficiently prevented by minimizing the thickness of the membrane layer [30]. Thus, preparing ultra-thin mixed matrix membrane layers as selective layers on top of the thick porous supports in multilayer composite structures can overcome this obstacle [7,31].

A number of approaches namely "thermal annealing" [32], "functionalization of fillers with silane coupling agents" [33], "loading and filler size adjustment" [34], "modification of fillers using ionic liquids" [35], and "polymer matrix grafting" [36] exist to overcome particle agglomeration in the polymer matrix. Ghadimi et al. modified the chemical surface of $SiO_2$ particles using cis-9-octadecenoic acid and added to PEBA 1657 polymeric matrix. The fabricated mixed matrix membrane revealed that $CO_2$ permeability and selectivity of $CO_2/N_2$ ($CH_4$) were 1.36 and 2.28 (2.25) fold higher than those associated with the neat PEBA membrane, respectively [27]. Shamsabadi et al. modified $TiO_2$ particles by grafting with 3-aminopropyl-diethoxymethylsilane (silane agent) and surface modification with carboxymethyl chitosan and fabricated PEBA 1657-modified $TiO_2$ mixed matrix membrane, which discloses higher $CO_2$ permeability and $CO_2/N_2$ selectivity of 60% and 33% than neat PEBA, respectively [36]. Mahdavi et al. added polyethylene glycol to the PEBA solution to improve the distribution of $\gamma$-$Al_2O_3$ particles in the polymer matrix. Their results revealed that $CO_2$ permeability and $CO_2/CH_4$ selectivity increased by 52% and 18%, respectively [29]. Despite the modification methods applied in the mentioned works to improve particle distribution in the PEBA matrix, particle loading could not increase higher than 8 wt.%.

According to $CO_2$ adsorption capacity measurements on $Al_2O_3$, this metal oxide can be a suitable selection for use as a filler in the preparation of mixed matrix membranes for $CO_2$ separation [19,20]. Thus, if $Al_2O_3$ particles are selected as embedded particles in the PEBA matrix, a new approach is proposed to overcome particle agglomeration at higher contents of these metal oxides.

The $Al_2O_3$ metal oxides can form at several phases through the phase transformation series of precursors $\rightarrow \gamma \rightarrow \delta \rightarrow \theta \rightarrow \alpha$-alumina. Among these phases, the alpha phase is a thermodynamically stable phase and creates particles with low tendency to agglomerate due to its small specific surface area and then, low surface energy [37]. In other words, due to low energy and high stability, $\alpha$-alumina particles have little tendency to come together and agglomerate, which is a reason for preventing the agglomeration of particles. Thus, we hypothesize that by applying the alpha phase of alumina particles, agglomeration of this metal oxide could be prevented. Then, the loading contents of these particles could considerably increase. This issue has never been raised and is new in this field.

This study prepared PEBA 1657-$\alpha$-$Al_2O_3$/PSf Multilayer Composite Mixed Matrix Membranes (MCMMMs) that PEBA 1657-$\alpha$-$Al_2O_3$ mixed matrix layer offered the main $CO_2$ separation properties. Alumina particles were used as a dispersed phase in the PEBA 1657 matrix for enhancing $CO_2$ uptake because of their strong affinity to $CO_2$ molecules. Moreover, the thermodynamically stable phase ($\alpha$ phase) of this metal oxide was selected to overcome particle agglomeration at the high contents of these particles. The loading of $\alpha$-$Al_2O_3$ particles in PEBA increased up to 30 wt.%, and this loading content for

all metal oxides has never been reported previously. A molecular simulation was also applied to clear the effect of $\alpha$-$Al_2O_3$ particles on polymer structure, solubility and diffusivity of gas molecules.

## 2. Experimental

### 2.1. Materials

PSf ultrafiltration membrane with Molecular Weight Cut Off (MWCO) of 10 kDa was purchased from Behta Water Inc. to be used as a support for the multilayer composite membrane. PEBA 1657 was provided from Arkema Inc. PEBA 1657 is a thermoplastic copolymer containing 60 wt.% of PEO chain and 40 wt.% of PA groups. Ethanol as a solvent for the preparation of a coating solution was supplied from Merck (99%). The $\alpha$-$Al_2O_3$ particles with an average size of 200 nm were purchased from Khuzestan Refractory Co. $CO_2$, $N_2$, and $CH_4$ gases were provided by Ehterami Gas services Company.

### 2.2. Membrane preparation

PEBA 1657/PSf multilayer composite membrane was prepared using the dip-coating method. A specific amount of PEBA 1657 was first dissolved in the solvent (ethanol/water = 70/30 wt.%) under reflux condition at 80°C for at least 2h to make 3 wt.% polymeric coating solution. The prepared solution was then cooled down to room temperature and poured into a coating dish. Next, PSf support was immersed in PEBA 1657 solution in a coating dish two times followed by drying at ambient temperature for 10 h after every coating time to achieve the final Multilayer Composite Neat Membrane (MCNM).

To prepare MCMMMs, different amounts of $\alpha$-$Al_2O_3$ particles were added to ethanol under stirring. The resulting suspensions were bath sonicated for 30 min and agitated for 1 h. Sonication and agitation steps were repeated two times. Afterward, calculated amounts of water and PEBA 1657 were added to the solution while stirring under reflux for 3 h at 80°C. The prepared solutions after sonicating for 15 min cooled down to room temperature and were poured into a coating dish. Finally, the PSf supports were immersed into prepared PEBA 1657-$\alpha$-$Al_2O_3$ solutions for two times with drying at ambient temperature for 10 h after every coating time to achieve final MCMMMs. Table 1 shows the membranes prepared in this research. The actual picture of the developed membrane (containing 20 wt.% alumina) is shown in Figure 1.

**Figure 1.** The actual picture of the developed membrane.

### 2.3. Characterizations

To characterize the chemical structure of the prepared membranes, Fourier Transforms Infrared spectroscopy (FTIR) was measured using an alpha-$p$ spectrometer (type Tensor 27, Bruker, Germany) equipped with a diamond attenuated total reflectance (ATR) crystal with a scanning range of 500–4000 $cm^{-1}$. The crystalline structure of the prepared membranes was identified by X-Ray Diffraction patterns (XRD, Siemens D5000, Germany). Bruker D8 ADVANCE X'Pert diffractometer was used to obtain XRD patterns using Cu-Ka radiation at 40 kV and 40 mA. The morphology and selective layer thickness of the prepared membranes were examined using a Scanning Electron Microscopy (SEM) apparatus (Cam Scan MV2300, LEO 440I, UK).

### 2.4. Gas permeation measurements

Gas permeation properties of the prepared membranes were measured using the flat plane module in a constant pressure/variable volume system.

The gas permeance ($J$) was calculated by Eq. (1) [9]:

$$J = \frac{Q}{A.\Delta P} \times \frac{273.15}{T} \times \frac{P}{76}, \quad (1)$$

where $Q$ ($cm^3/s$) is the flow rate of permeated gas, $A$ ($cm^2$) is the effective membrane area, $P$ (cmHg) is the pressure, $T$ (K) is the absolute temperature, and $\Delta P$ (cmHg) is the transmembrane pressure. The unit of permeance is denoted in SI units ($mol.m^{-2}$

**Table 1.** Abbreviation of the prepared membranes.

| Prepared membranes | Abbreviation |
|---|---|
| PEBA 1657(3 wt.%)/PSf | MCNM |
| PEBA 1657(3 wt.%) + $\alpha$-$Al_2O_3$ (10 wt.%)/PSf | MCMMM10 |
| PEBA 1657(3 wt.%) + $\alpha$-$Al_2O_3$ (20 wt.%)/PSf | MCMMM20 |
| PEBA 1657(3 wt.%) + $\alpha$-$Al_2O_3$ (30 wt.%)/PSf | MCMMM30 |

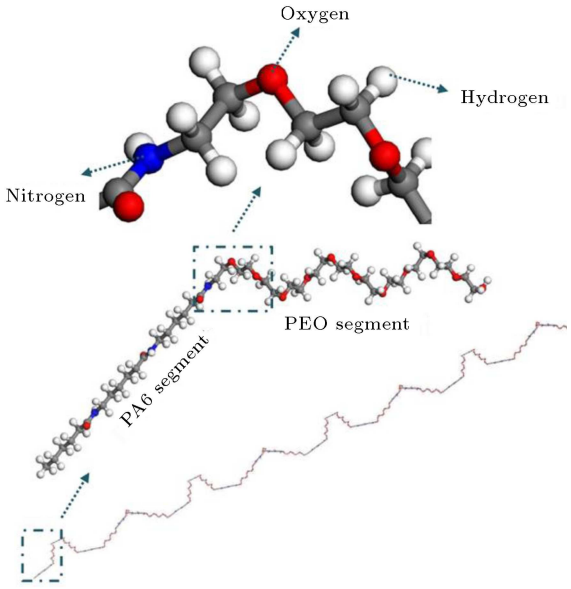


**Figure 2.** Configuration of PEBA 1657 polymer chain.

$s^{-1}Pa^{-1}$) (mol.$m^{-2}$ $s^{-1}Pa^{-1}$ = 2.985 × $10^3$ $cm^3$ (STP)/ ($cm^2$.s.cmHg)).

The ideal selectivity ($\alpha_{A/B}$) for a pair of gases is defined as their permeance ratio [9]:

$$\alpha_{AB} = J_A/J_B. \quad (2)$$

### 2.5. Molecular simulation

The molecular simulation was conducted using Material Studio 8.0 software. Molecular Dynamics (MD) and Grand Canonical Monte Carlo (GCMC) simulations were employed to explore the effect of $\alpha$-$Al_2O_3$ on the separation performance of PEBA.

In this simulation, a modified form of Condensed-phase Optimized Molecular Potential for Atomistic Simulation Studies II (COMPASS II) force field was used to simulate gas separation in membranes with cut-off distance of 10 Å. As shown in Figure 2, the PEBA chain with 20 super units was utilized to construct simulation cells of pure PEBA and mixed matrix membranes. Simulation cells were built by 20 output frames with an initial density of 0.6 g/$cm^3$. The simulated cells are 6-sided and 10 gas molecules are used in the membrane cells. After energy minimization and geometry optimization of prepared cells, 1 ns NPT run under the pressure of 1 bar and at a temperature of 298 K was applied to reach equilibrium density and obtain the ideal structure of the amorphous cells. Afterward, 2.5 ns NVT simulation was performed to investigate the detailed motion of gas molecules in constructed cells. The time step was selected 5 ps.

## 3. Results and discussion

### 3.1. Morphology of membranes

Figure 3 shows the surface and cross-sectional morphologies of MCNM and MCMMMs with 5, 10, 20, and 30 wt.% $\alpha$-$Al_2O_3$ loadings. From the top surface schema of MCNM and MCMMMs, no apparent holes or defects can be seen at these magnifications and the formed selective layers are quite dense. Based on Figure 3(a″)–(d″), the surface morphology of MCNM is smooth and homogeneous, while the addition of $\alpha$-$Al_2O_3$ particles led to an increase in the surface roughness of the MCMMMs compared to the MCNM. Besides, as can be seen in Figure 3(d″), at higher loading (30 wt.%) of particles, the $\alpha$-$Al_2O_3$ particles agglomerated in the selective layer matrix.

The cross-sectional morphologies of the MCNM and MCMMMs (Figure 3(a)–(d)) indicate that the prepared membranes consist of the PEBA selective layer, the finger-like PSf layer, and non-woven fabric polyester sub-layer. As can be seen in Figure 3(a′)–(d′), the thickness of PEBA selective layers in all the prepared membranes is skinny with thickness on the submicron scale (less than 1 $\mu$m). Moreover, according to the mentioned figures, the excellent adhesion of the PEBA selective layer and the PSf support is visible in all the prepared membranes.

### 3.2. Crystalline structure of membranes

To study the crystalline structure of the prepared membranes, XRD analysis was used. The XRD patterns of the MCNM and MCMMMs are shown in Figure 4. Considering the diffraction patterns of MCNM, it is clear that PEBA 1657 has a semi-crystalline structure due to weak and strong diffraction peaks at different values of 2$\theta$ angles. The weak diffraction peaks at 15° and 18° of 2$\theta$ are related to the amorphous section and the sharp peaks at 23°, 26°, and 29° are attributed to the crystalline section of the PEBA 1657 matrix. Based on Figure 4, XRD patterns of MCMMMs reveal that in the membranes with loadings of 20 and 30 wt.% filler, not only a new peak appeared at around 14° but also the intensity of diffraction peaks at crystalline and amorphous sections increased. These findings indicate that high loadings of $\alpha$-$Al_2O_3$ particles enhanced their crystalline nature and attenuated the amorphous nature of PEBA 1657; this behavior is more noticeable for the membrane with 20 wt.% loading of filler due to the proper distribution of $\alpha$-$Al_2O_3$ particles in the polymer matrix than the sample with a 30 wt.% loading of filler. Since the crystalline structure of the membrane has a considerable effect on gas diffusivity in polymeric membranes, a decrease in gas diffusivity through the MCMMMs is expected due to the enhanced crystalline structure of polymer matrix. In nonporous membranes with solution-diffusion transport mechanism, the reduction of gas diffusivity confirms the selectivity of the membrane due to the reduced permeability of insoluble gases, which can transport through the membrane by

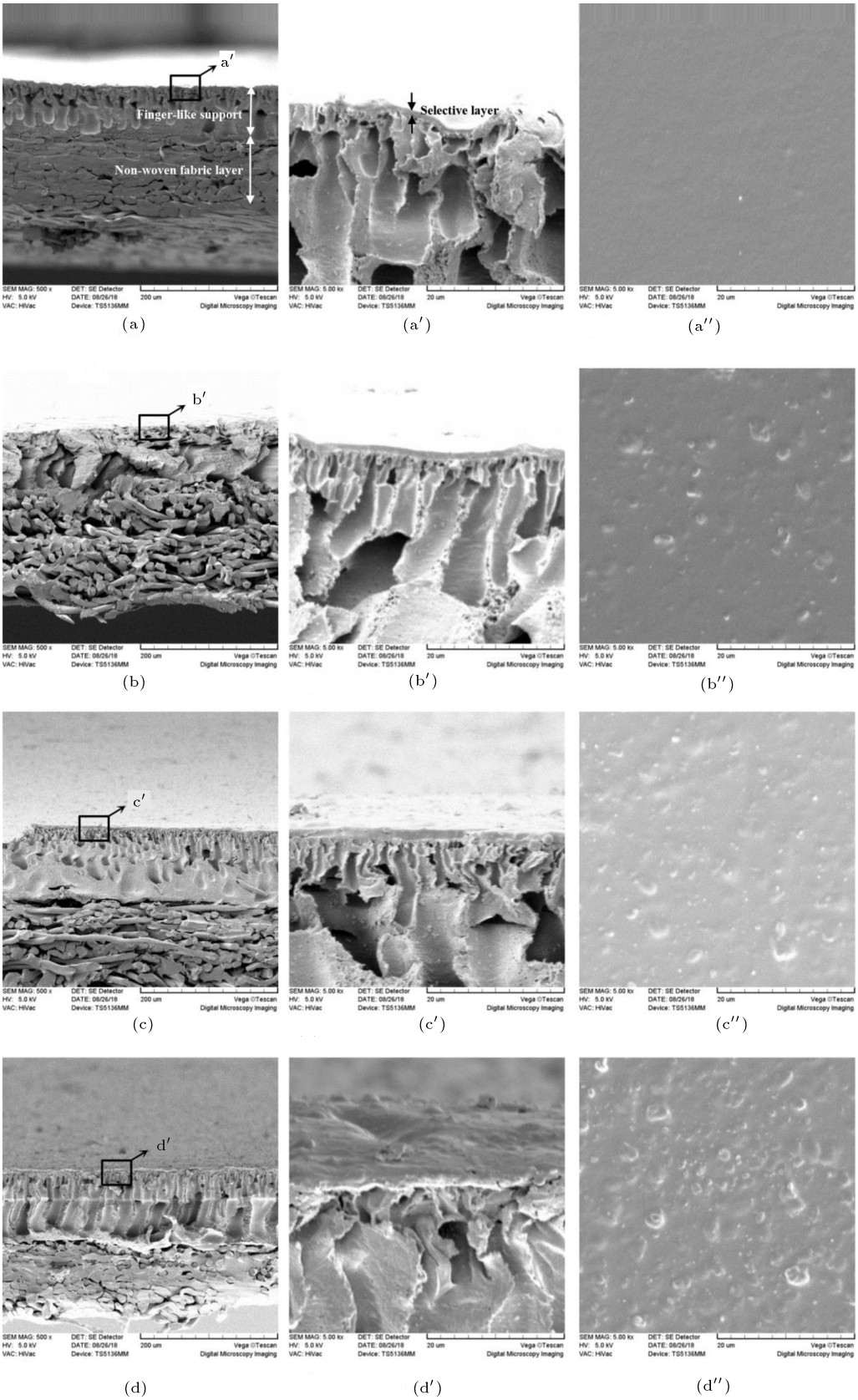


**Figure 3.** SEM images of surface and cross-sections of membranes with different magnifications. MCNM: (a), (a′) cross-section, and (a″) surface; MCMMM10: (b), (b′) cross-section, and (b″) surface; MCMMM20: (c), (c′) cross-section, and (c″) surface; MCMMM30: (d), (d′) cross-section, and (d″) surface.

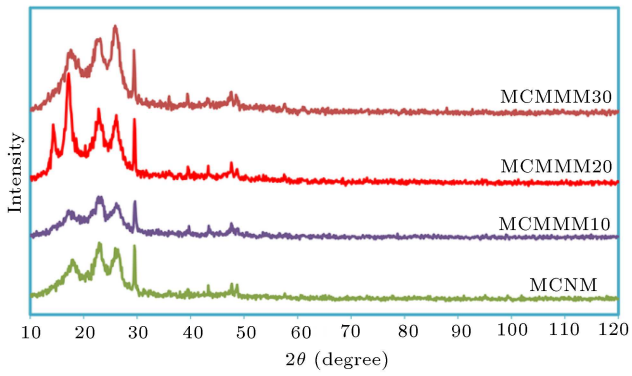


**Figure 4.** XRD patterns for MCNM and MCMMMs.

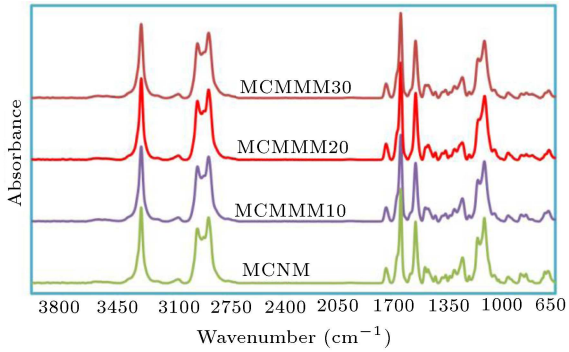


**Figure 5.** FTIR spectra for MCNM and MCMMMs.

diffusion mechanism. This behavior is confirmed by gas permeation measurements.

### 3.3. Chemical structure of membranes

FTIR spectra are also employed to study the chemical structure of polymer chains in MCNM and MCMMMs, as shown in Figure 5. In the MCNM, the observed peak at 1020–1180 $cm^{-1}$ is attributed to C–O–C bonds in the soft segment part of PEBA (polyethylene oxide (PEO) part) [11]. The peak at 3299 $cm^{-1}$ is assigned to –N–H– linkages, while the observed peaks at 1637 and 1733 $cm^{-1}$ indicate the existence of the two types of amide and ester groups, C=O, in PEBA. It is noteworthy that the above three functional groups indicate the presence of the hard segment of PEBA (polyamide (PA) part). Moreover, C–OH and aliphatic C–H groups display characteristic peaks at 1544 and 2800–2977 1540 $cm^{-1}$, respectively [25,38].

Figure 5 shows that after the addition of $\alpha$-$Al_2O_3$ particles to the PEBA 1657 matrix, no new characteristic peak was found, indicating that there was no strong chemical interaction between $\alpha$-$Al_2O_3$ particles and PEBA chains. There are some differences between the FTIR spectra of the MCNM and MCMMMs. The precise exploration reveals that the peak intensity at 1020–1059 $cm^{-1}$ increased, which was related to the PEO soft segment part of PEBA. Moreover, the intensity of peaks at 3299, 1637, and 1733 $cm^{-1}$ increased as the characteristic peaks of the PA hard segment of PEBA. These changes in MCMMMs indicate that a hydrogen bond was developed between PEO and PA segments of PEBA, leading to the enhancement of crystalline nature of the polymer [22,35].

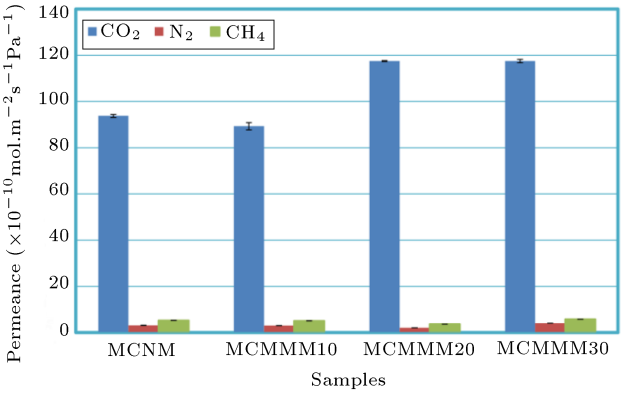


**Figure 6.** The permeances of $CO_2$, $CH_4$, and $N_2$ for MCNM and MCMMMs at 25°C and 7 bar.

### 3.4. Gas permeation performance of membranes

In this study, a constant feed pressure system is applied to gas permeation tests. The permeance of three gases ($CO_2$, $N_2$, and $CH_4$) was measured at 25°C and pressure of 7 bar. Figure 6 indicates the effect of particles loading on the permeances of gases. As can be seen in this figure, in all the prepared membranes, $CO_2$ permeance is higher than that of other gases. Regarding the solution-diffusion primary mechanism in nonporous membranes, the reasons for high permeance of $CO_2$ in comparison to other ones can be justified by higher condensation coefficient, higher polarizability, and lower kinetic diameter of this gas. The permeance results presented in Table 2 reveal that in the MCMMMs with high loadings (20 and 30 wt.%)

**Table 2.** The permeance of different gases in the prepared membranes (25°C and 7 bar).

| Membrane | $P_{CO_2}$ ($\times 10^{-10}$ mol.m$^{-2}$ s$^{-1}$Pa$^{-1}$) | $P_{CH_4}$ ($\times 10^{-10}$ mol.m$^{-2}$ s$^{-1}$Pa$^{-1}$) | $P_{N_2}$ ($\times 10^{-10}$ mol.m$^{-2}$ s$^{-1}$Pa$^{-1}$) |
|---|---|---|---|
| MCNM | 93.77 ± 0.60 | 5.25 ± 0.03 | 3.07 ± 0.05 |
| MCMMM10 | 89.30 ± 0.17 | 5.05 ± 0.02 | 2.99 ± 0.01 |
| MCMMM20 | 117.50 ± 0.71 | 3.62 ± 0.02 | 2.06 ± 0.02 |
| MCMMM30 | 117.50 ± 4.95 | 5.74 ± 0.01 | 4.00 ± 0.02 |

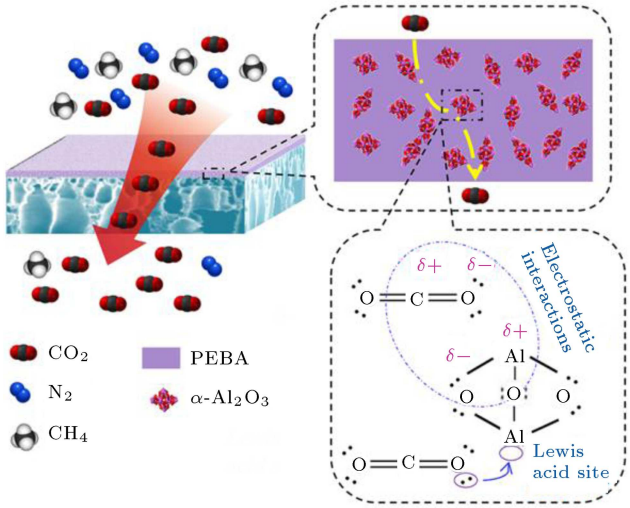


**Figure 7.** Schematic illustration of gas permeation through the prepared MCMMMs.

of $\alpha$-$Al_2O_3$ particles, $CO_2$ permeance is 25% higher than that of MCNM because the membrane permeance at high loadings is controlled by solubility rather than diffusivity.

As mentioned earlier, the transport mechanism of gas through the prepared nonporous selective layer membranes is described by the solution-diffusion model. The gases solubilize into the surface of the membrane selective layer on the feed side, diffuse across the membrane matrix, and subsequently desorb on the permeate side [39].

The gas permeance coefficient ($P_A$) can be defined by Eq. (3) [40,41]:

$$P_A = \frac{S_A \times D_A}{l}, \tag{3}$$

where $S_A$ is the gas solubility coefficient, $D_A$ the average effective diffusion coefficient and $l$ the membrane thickness [40,41].

As confirmed by XRD and FTIR results, the high loadings of $\alpha$-$Al_2O_3$ particles induced an enhancement in the crystalline nature of PEBA, leading to the reduction of molecules diffusivity in MCMMMs. However, $CO_2$ diffusivity decreased, while its solubility significantly increased and could overcome the decreased diffusivity, leading to increased $CO_2$ permeance at high loadings of $\alpha$-$Al_2O_3$ particles.

It is worth noting that increase in $CO_2$ solubility results from the enhancement of membrane affinity for $CO_2$ molecules which can be attributed to the two following reasons (see Figure 7): (1) Electrostatic interactions between $CO_2$ and $\alpha$-$Al_2O_3$ particles and (2) The existing interaction between Lewis acid sites of $\alpha$-$Al_2O_3$ particles and $CO_2$ molecules.

Figure 8 shows the ideal selectivity of $CO_2/CH_4$ and $CO_2/N_2$ for all the prepared membranes. As can be seen in this figure, the MCMMM20 exhibits superior

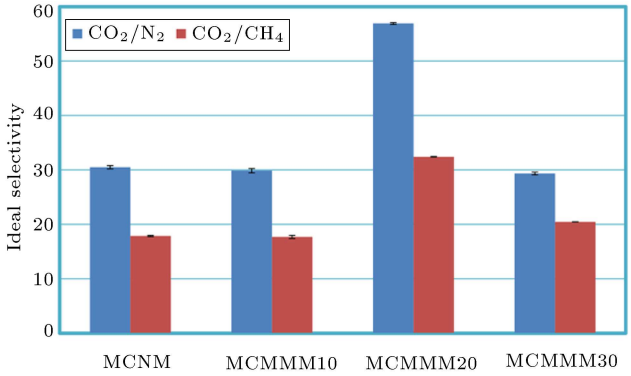


**Figure 8.** $CO_2/CH_4$ and $CO_2/N_2$ ideal selectivity of MCNM and MCMMMs at 25°C and 7 bar.

ideal selectivity of $CO_2/CH_4$ and $CO_2/N_2$ compared to MCNM. The optimum loading (20 wt.%) and the ideal selectivity of $CO_2/CH_4$ and $CO_2/N_2$ are 81.5% and 86.5% higher than those of MCNM, respectively.

The ideal selectivity can be expressed as the product of solubility selectivity and diffusivity selectivity as follows [42,43]:

$$\alpha_{A/B} = \frac{D_A}{D_B} \times \frac{S_A}{S_B}. \tag{4}$$

The solubility selectivity is affected by the interactions among polymer chains, gas molecules, and gas condensability, whereas the diffusivity selectivity depends on the rigidity of the polymer chains and the size of the gas molecules [39]. The main contribution of $\alpha$-$Al_2O_3$ particles in improving the ideal selectivity of $CO_2/CH_4$ and $CO_2/N_2$ in MCMMMs is by enhancing both the solubility selectivity and the diffusivity selectivity sections of ideal selectivity.

In fact, increasing the ideal selectivity of $CO_2/CH_4$ and $CO_2/N_2$ in MCMMMs is mainly owing to the two following reasons. First, incorporation of $\alpha$-$Al_2O_3$ particles enhanced the crystalline nature of PEBA, as confirmed by XRD and FTIR analyses. This phenomenon decreases the diffusivity of $CH_4$ and $N_2$ more than that of $CO_2$ due to the higher kinetic diameter of these gases than $CO_2$ and results in high diffusivity selectivity of MCMMMs in comparison with MCNM. Second, the high loading of $\alpha$-$Al_2O_3$ particles remarkably increased the membrane affinity for $CO_2$ followed by higher uptake of this gas in the membrane matrix. Increasing $CO_2$ solubility leads to significant improvement in the solubility selectivity of MCMMMs in comparison with MCNM.

As shown in Figure 8, the ideal selectivity of $CO_2/CH_4$ and $CO_2/N_2$ for the MCMMM30 is lower than that for MCMMM20 due to the agglomeration of $\alpha$-$Al_2O_3$ particles in selective layer matrix confirmed by surface SEM morphologies. The agglomeration of particles in MCMMM30 inhibits the enhancement of polymer crystalline nature (see Figure 5) and in-

creases the diffusivity of $CO_2$, $CH_4$, and $N_2$ gases simultaneously. Therefore, not only the permeance of $CO_2$ for MCMMM30 increases, but also the permeance of $CH_4$ and $N_2$ for this membrane increases (see Figure 6), hence lower ideal selectivity of $CO_2/CH_4$ and $CO_2/N_2$ for MCMMM30 in comparison with these ideal selectivities for MCMMM20.

### *3.5. Molecular simulation results*

To investigate the effect of $Al_2O_3$ particles on polymer structure and solubility and diffusivity of gas molecules, the constructed amorphous cells are given in Figure 9.

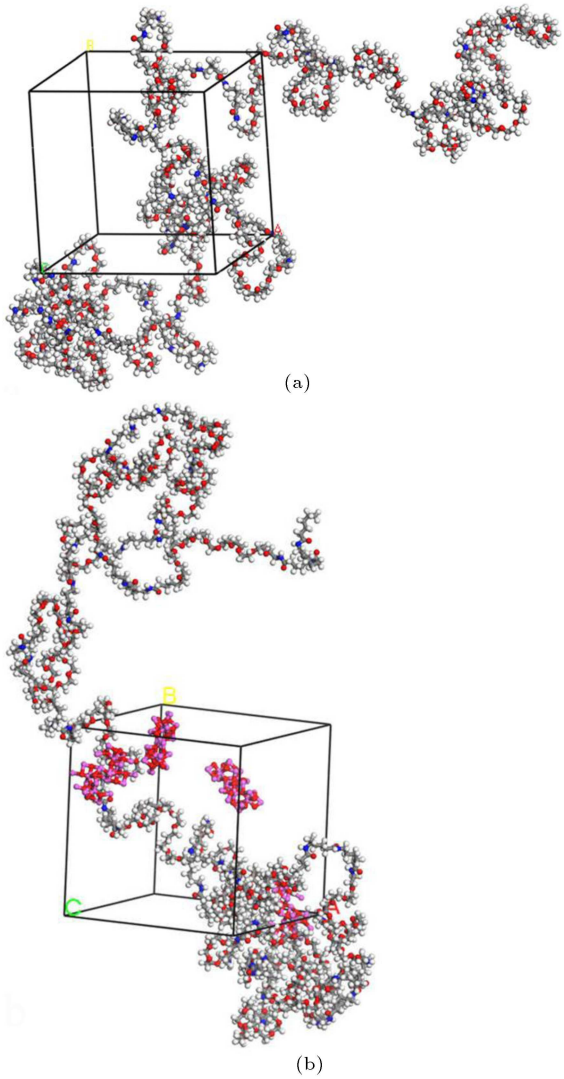


**Figure 9.** Configuration of constructed amorphous cells: (a) MCNM and (b) MCMMM20.

The calculated average density values and the radius of gyration ($R_g$) for simulated MCNM and MCMMM20 membranes are presented in Table 3. According to this table, the average density of the simulated neat PEBA membrane is very close to experimental data, indicating the high accuracy of the simulation procedure. $R_g$ is utilized to characterize the dimensions of the PEBA chains [45]. This value decreases upon adding $Al_2O_3$ to the PEBA matrix, which indicates that the addition of $Al_2O_3$ particles affects the structure of the polymer and the interaction between these particles and PEBA chains, leading to the increased crystalline nature of this polymer as confirmed previously in experimental results. The calculated cell volume, free volume, occupied volume, and Fractional Free Volume (FFV) of the simulated membranes are presented in Table 4. According to this table, the FFV of the membrane decreases with the addition of $Al_2O_3$ particles to the PEBA matrix, which is due to the polymer chain packing with increasing particle loading. Figure 10 illustrates the simulation cells of MCNM and MCMMM20, showing their free volumes in blue color.

The solubility and diffusivity of $CO_2$ molecules were obtained by the Metropolis method in the GCMC ensemble [47,48]. The calculated solubility and diffusivity are reported in Table 5. According to this table, $CO_2$ diffusivity decreased by incorporating $Al_2O_3$ particles in the PEBA matrix, which is due to the enhanced crystalline nature and reduced free volume of the membrane. Moreover, it can be confirmed that $CO_2$ solubility significantly increased by adding $Al_2O_3$ to the PEBA matrix due to the electrostatic interactions between $CO_2$ and $Al_2O_3$ particles and role of aluminum sites of $Al_2O_3$ as Lewis acid sites and their high affinity to $CO_2$ molecules. To explore this behavior and investigate the importance of aluminum and oxygen atoms of $Al_2O_3$ in the solubility of $CO_2$ molecules, the Radial Distribution Function (RDF) is calculated. As can be seen in Figure 11, the RDF peak at $r = 3.87$ Å for $CO_2$ molecules and aluminum atoms indicates the strong interaction between $CO_2$ molecules and aluminum atoms in comparison with oxygen atoms. This behavior is attributed to this fact that the Al atoms not only have electrostatic interactions with $CO_2$ molecules but also play as absorptive Lewis acid sites for $CO_2$ molecules.

The location of adsorbed $CO_2$ molecules within the neat and filled PEBA membranes is shown in

**Table 3.** The average density and radius of gyration for simulated membranes.

| Membrane | Simulated average density (g/cm$^3$) | Simulated $R_g$ (Å) |
|---|---|---|
| MCNM | 1.11 (1.14[a]) | 27.84 |
| MCMMM20 | 1.31 | 9.49 |

[a]Experimental result [44].

**Table 4.** The simulation cell volume, the free volume, the occupied volume, and the Fractional Free Volume (FFV) of the simulated membranes.

| Membrane | Cell volume ($Å^3$) | Free volume ($Å^3$) | Occupied volume ($Å^3$) | FFV ($Å^3$) |
|---|---|---|---|---|
| MCNM | 24801.45 | 2978.57 | 21822.88 | 0.12 (0.13[a]) |
| MCMMM20 | 25660.65 | 2199.20 | 23461.45 | 0.09 |

[a]Experimental result [46].

**Table 5.** Solubility and diffusivity of $CO_2$ molecules for simulated membranes.

| Membrane | $CO_2$ solubility[a] ($\times 10^{-4}$ $cm^3$ (STP) $cm^{-3}$ (polymer) $cmHg^{-1}$) | $CO_2$ diffusivity ($\times 10^{-6}$ $cm^2/s$) |
|---|---|---|
| MCNM | 167 | 0.97 |
| MCMMM20 | 570 | 0.36 |

[a]The final solubility is the average of seven sorption isotherms.

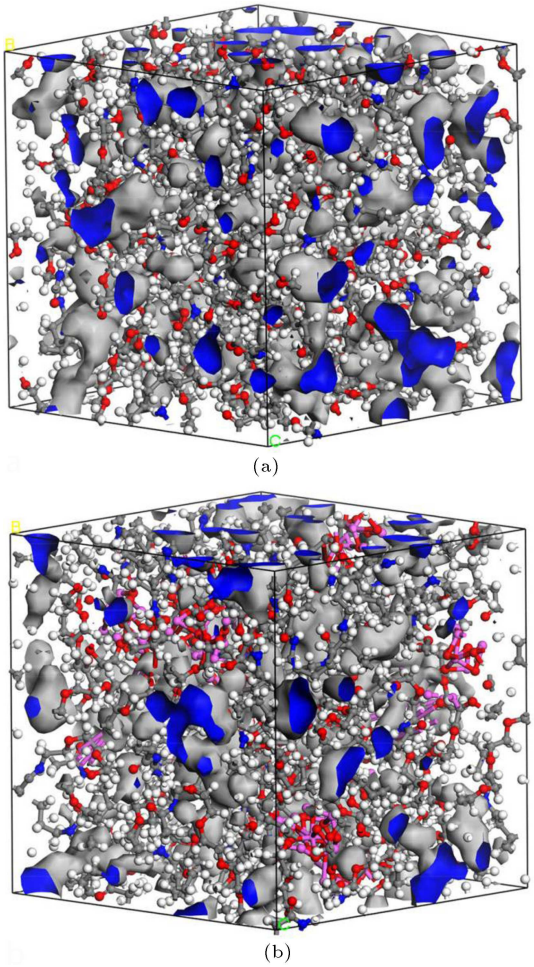

**Figure 10.** Schematic illustration of free volume (blue color) for constructed amorphous cells: (a) MCNM and (b) MCMMM20.

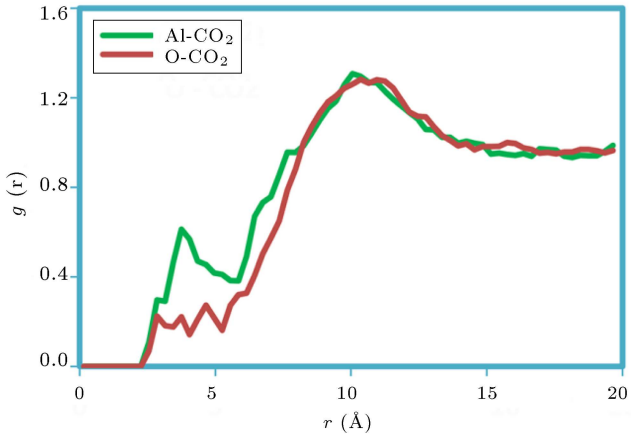


**Figure 11.** The RDF for the interaction of $CO_2$ with Al and O atoms of $Al_2O_3$.

Figure 12. As can be seen in this figure, the number of adsorption sites for $CO_2$ increases by adding $Al_2O_3$ particles to PEBA structure. According to Figure 13, the $CO_2$ molecules are adsorbed in the surrounding of the $Al_2O_3$ particles more than other areas, indicating the high affinity of these particles to adsorb $CO_2$ molecules on their sites. These results show that $Al_2O_3$ particles could be exceedingly helpful in enhancing $CO_2$ solubility in the mixed matrix membrane.

### *3.6. Comparison with other studies*

Table 6 indicates selective layer thicknesses, $CO_2$ permeance, and $CO_2/CH_4$ and $CO_2/N_2$ ideal selectivities for the MCMMM20 in comparison with membranes containing modified particles in other studies. As can be seen in this table, the MCMMM20 has good permeance and ideal selectivities for the $CO_2$ gas over $CH_4$ and $N_2$, which is comparable with the separation performance of other membranes containing modified particles. It is worth noting that the modification of particles is complicated and costly, while this work could exceptionally improve PEBA performance with no particle modification. Among other studies, this work demonstrates that the MCMMM20 could be a potential candidate for the separation of carbon dioxide from flue gas and natural gas and make the membranes economically attractive for industrial applications.

**Table 6.** Gas permeation performance of different PEBA based membranes.

| Membrane | Selective layer thickness ($\mu$m) | $CO_2$ permeance ($\times 10^{-10}$ mol. $m^{-2}$ $s^{-1}Pa^{-1}$) | $CO_2/CH_4$ | $CO_2/N_2$ | Ref. |
|---|---|---|---|---|---|
| PEI-DA modified $TiO_2$-PEBA/PVDF | 10 | 25.11 | - | 101 | [19] |
| Imidazolium modified ZIF-8-PEBA/PES | 11.3 | 77.04 | 37 | 70 | [42] |
| APTES modified ZIF8-PEBA/PES | 2.8 | 679.74 | 15.9 | - | [43] |
| APTMS modified ZIF8-PEBA/PES | 3.4 | 619.47 | 14.5 | - | [43] |
| $NH_2$ modified UiO-66-PEBA/PVDF | 11 | 26.48 | - | 66.1 | [44] |
| MCMMM20 | 1 | 117.50 | 32.41 | 56.9 | This work |

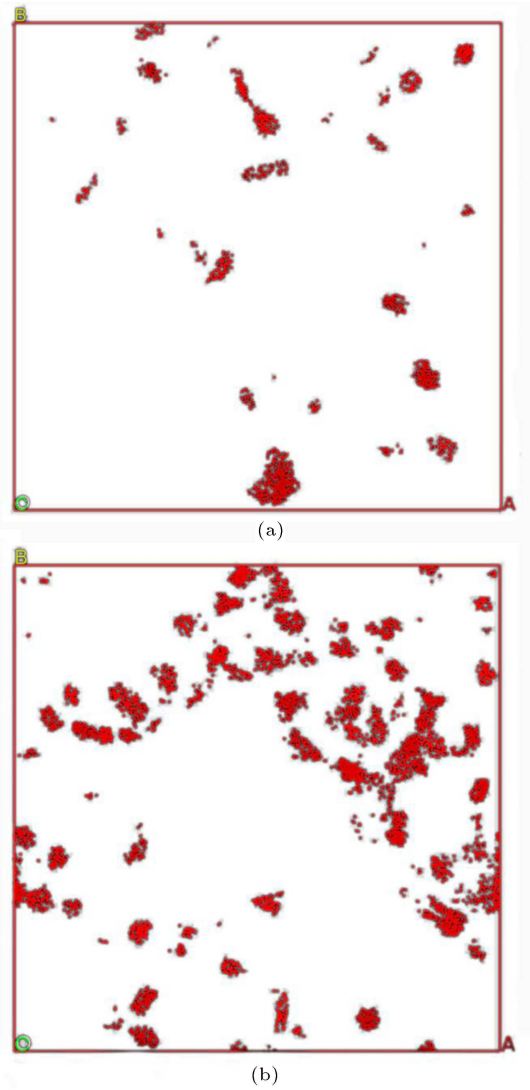


**Figure 12.** The location of adsorbed $CO_2$ molecules (red points) within constructed membranes: (a) MCNM and (b) MCMMM20.

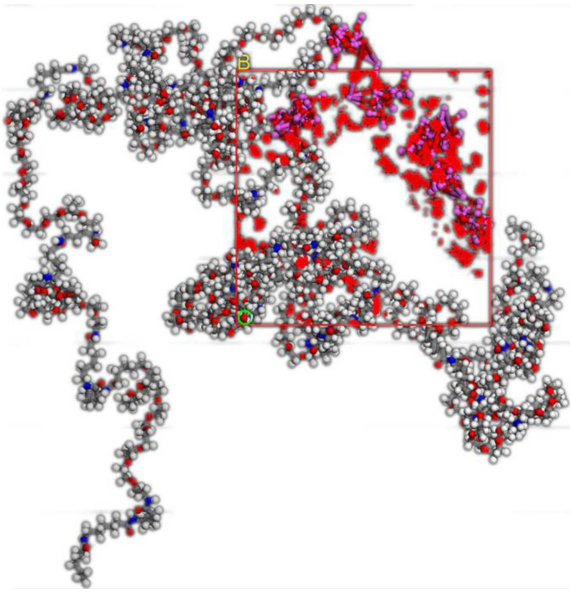


**Figure 13.** The location of adsorbed $CO_2$ molecules (red points) in the surrounding area of the PEBA matrix and $\alpha$-$Al_2O_3$ particles in MCMMM20.

## 4. Conclusion

In this study, Polyether Block Amide (PEBA) 1657-$\alpha$-$Al_2O_3$/PSf Multilayer Composite Mixed Matrix Membranes (MCMMMs) with different loadings of $\alpha$-$Al_2O_3$ particles were prepared for $CO_2$ separation. The prepared membranes were characterized using Scanning Electron Microscopy (SEM), X-Ray Diffraction (XRD), Fourier Transforms Infrared spectroscopy (FTIR), and gas permeation analyses. The results displayed that the application of the alpha phase of the $Al_2O_3$ particles reduced the agglomeration of fillers and could increase particle loading up to 30 wt.%. Moreover, the $\alpha$-$Al_2O_3$ particles not only considerably increase $CO_2/CH_4$ and $CO_2/N_2$ selectivity of PEBA layers (81.5% and 86.5%, respectively) but also improve the $CO_2$ permeance (25%) due to the electrostatic interactions between $CO_2$ and $\alpha$-$Al_2O_3$ particles and the role of Lewis acid sites of $\alpha$-$Al_2O_3$ as the absorptive sites for $CO_2$ molecules. It should be noted that the ideal selectivity of $CO_2/CH_4$ and $CO_2/N_2$ was improved due to the enhancement of both solubility selectivity and diffusivity selectivity. The XRD and FTIR analyses demonstrated that diffusivity selectivity increased because of the enhanced crystalline nature of PEBA, whereas the solubility selectivity was enhanced by increasing the solubility of $CO_2$ in a selective mixed matrix layer.

The molecular simulation like experimental re-

sults proved the enhancement of crystalline nature and reduction of free volume of the polymer by adding $Al_2O_3$ particles, which reduced the diffusivity of $CO_2$ molecules. Moreover, the Grand Canonical Monte Carlo (GCMC) method indicated that the $Al_2O_3$ particles significantly increased the $CO_2$ uptake of the membrane (241%) by creating a strong affinity to $CO_2$ molecules. The experimental and simulation studies proved that $\alpha$-$Al_2O_3$ could be a right candidate for improving the PEBA performance for $CO_2$ separation.

## References


1. Ilyas, A., Muhammad, N., and Amjad, M. "Effect of zeolite surface modification with ionic liquid [APTMS][Ac] on gas separation performance of mixed matrix membranes", *Sep Purif Technol.*, **205**, pp. 176–183 (2018). https://doi.org/10.1016/j.seppur.2018.05.040.

2. Azizi, N., Mahdavi, HR., Isanejad, M., et al. "Effects of low and high molecular mass PEG incorporation into different types of poly(ether-b-amide) copolymers on the permeation properties of $CO_2$ and $CH_4$", *J Polym Res.*, **24**, p. 141 (2017). https:// 10.1007/s10965-017-1297-1.

3. Tu, Z., Liu, P., Zhang, X., et al. "Highly-selective separation of $CO_2$ from $N_2$ or $CH_4$ in task-specific ionic liquid membranes: Facilitated transport and salting-out effect", *Sep. Purif. Technol.*, **254**, pp. 1–9 (2021). https://doi.org/10.1016/j.seppur.2020.117621.

4. Fan, Y., Yu, H., Xu, S., et al. "Zn(II)-modified imidazole containing polyimide/ZIF-8 mixed matrix membranes for gas separations", *J. Memb. Sci.*, **597**, 117775 (2020). https://doi.org/10.1016/j.memsci.2019.117775.

5. Yoon, K.W., Kim, H., Kang, Y.S., et al. "1-Butyl-3-methylimidazolium tetrafluoroborate/zinc oxide composite membrane for high $CO_2$ separation performance", *Chem Eng J.*, **320**, pp. 50–54 (2017). https://doi.org/10.1016/j.cej.2017.03.026.

6. Kanehashi, S., Aguiar, A., Lu, H.T., et al. "Effects of industrial gas impurities on the performance of mixed matrix membranes", *J Membr Sci.*, **549**, pp. 686–692 (2018). https://doi.org/10.1016/j.memsci.2017.10.056.

7. Asghari, M., Mosadegh, M., and RiasatHarami, H. "Supported PEBA-zeolite 13X nano-composite membranes for gas separation: Preparation, characterization and molecular dynamics simulation", *Chem Eng Sci*, **187**, pp. 67–78 (2018). https://doi.org/10.1016/j.ces.2018.04.067.

8. Jiang, Y., Liu, C., Caro, J., et al. "A new UiO-66-$NH_2$ based mixed-matrix membranes with high $CO_2/CH_4$ separation performance", *Microporous Mesoporous Mater*, **274**, pp. 203–211 (2019). https://doi.org/10.1016/j.micromeso.2018.08.003.

9. Karamouz, F., Maghsoudi, H., and Yegani, R. "Synthesis and characterization of high permeable PEBA membranes for CO2/CH4 separation", *J Nat Gas Sci Eng*, **35**, pp. 980–985 (2016). https://doi.org/10.1016/j.jngse.2016.09.036.

10. Momeni, M., Kojabad, M.E., Khanmohammadi, S., et al. "Impact of support on the fabrication of poly (ether-b-amide) composite membrane and economic evaluation for natural gas sweetening", *J Nat Gas Sci Eng*, **62**, pp. 236–246 (2019). https://doi.org/10.1016/j.jngse.2018.12.014.

11. Azizi, N., Mohammadi, T., and Behbahani, R.M. "Synthesis of a new nanocomposite membrane (PEBAX-1074/PEG-400/$TiO_2$) in order to separate $CO_2$ from $CH_4$", *J Nat Gas Sci Eng*, **37**, pp. 39–51 (2017). https://doi.org/10.1016/j.jngse.2016.11.038.

12. Ghasemi, E., Omidkhah, M., and Ebadi, A. "Preparation and characterization of novel Ionic liquid/Pebax membranes for efficient $CO_2$/light gases separation", *J Ind Eng Chem*, **5**, pp. 77–89 (2017). http://dx.doi.org/10.1016/j.jiec.2017.02.017.

13. Ghadimi, A., Amirilargani, M., Mohammadi, T., et al. "Preparation of alloyed poly(ether block amide)/poly(ethylene glycol diacrylate) membranes for separation of $CO_2/H_2$(syngas application)", *J Membr Sci*, **458**, pp. 14–26 (2014). https://doi.org/10.1016/j.memsci.2014.01.048.

14. Samarasinghe, S.A.S.C., Chuah, C.Y., Yang, Y., et al. "Tailoring $CO_2/CH_4$ separation properties of mixed-matrix membranes via combined use of two- and three-dimensional metal-organic frameworks", *J Membr Sci.*, **557**, pp. 30–37 (2018). https://doi.org/10.1016/j.memsci.2018.04.025.

15. Li, W., Samarasinghe, S.A.S.C., and Bae, T. "Enhancing $CO_2/CH_4$ separation performance and mechanical strength of mixed-matrix membrane via combined use of graphene oxide and ZIF-8", *J Ind Eng Chem.*, **67**, pp. 156–163 (2018). https://doi.org/10.1016/j.jiec.2018.06.026.

16. Hwang, S., Seok, W., Jin, S., et al. "Hollow ZIF-8 nanoparticles improve the permeability of mixed matrix membranes for $CO_2/CH_4$ gas separation", *J Membr Sci.*, **480**, pp. 11–19 (2015). https://doi.org/10.1016/j.memsci.2015.01.038.

17. Zhang, X., Zhang, T., Wang, Y., et al. "Mixed-matrix membranes based on Zn/Ni-ZIF-8-PEBA for high performance $CO_2$ separation", *J Membr Sci.*, **560**, pp. 38–46 (2018). https://doi.org/10.1016/j.memsci.2018.05.004.

18. Jomekian, A., Bazooyar, B., Mosayebi, R., et al. "Ionic liquid-modified Pebax® 1657 membrane filled by ZIF-8 particles for separation of $CO_2$ from $CH_4$, $N_2$ and $H_2$", *J Membr Sci.*, **524**, pp. 652–662 (2017). https://doi.org/10.1016/j.memsci.2016.11.065.

19. Yong, Z., Mata, V., and Rodrigues, A.E. "Adsorption of carbon dioxide on basic alumina at high temperatures", *J Chem Eng. Data*, **45**, pp. 1093–1095 (2000). https://doi.org/10.1021/je000075i.

20. Esmaili, J. and Ehsani, M.R. "Study on the effect of preparation parameters of $K_2CO_3/Al_2O_3$ sorbent on $CO_2$ capture capacity at flue gas operating conditions", *J Encapsulation Adsorpt Sci*, **3**, pp. 57–63 (2013). https://doi.org/10.4236/jeas.2013.32007.

21. Matteucci, S.T. "Gas transport properties of reverse selective nanocomposite materials", University of Texas, Austin, United States (2007). http://hdl.handle.net/2152/3631.

22. Azizi, N., Mohammadi, T., and Behbahani, R.M. "Comparison of permeability performance of PEBAX-1074/$TiO_2$, PEBAX-1074/$SiO_2$ and PEBAX-1074/$Al_2O_3$ nanocomposite membranes for $CO_2/CH_4$ separation", *Chem. Eng. Res. Des.*, **117**, pp. 177–189 (2017). https://doi.org/10.1016/j.cherd.2016.10.018.

23. Zhu, H., Yuan, J., Zhao, J., et al. "Enhanced $CO_2/N_2$ separation performance by using dopamine/polyethyleneimine-grafted $TiO_2$ nanoparticles filled PEBA mixed-matrix membranes", *Sep Purif Technol.*, pp. 78–86 (2019). https://doi.org/10.1016/j.seppur.2018.02.020.

24. Song, C., Li, R., Fan, Z., et al. "$CO_2/N_2$ separation performance of Pebax /MIL-101 and Pebax /NH2 - MIL- 101 mixed matrix membranes and intensi fication via sub-ambient operation", *Sep. Purif. Technol.*, **238**, 116500 (2020). https://doi.org/10.1016/j.seppur.2020.116500.

25. Azizi, N., Mohammadi, T., and Behbahani, R.M. "Synthesis of a PEBAX-1074/ZnO nanocomposite membrane with improved $CO_2$ separation performance", *J Energy Chem.*, **26**, pp. 454–465 (2017). https://doi.org/10.1016/j.jechem.2016.11.018.

26. Asghari, M., Sheikh, M., and Dehghani, M. "Comparison of ZnO nanofillers of different shapes on physical, thermal and gas transport properties of PEBA membrane: experimental and molecular simulation", *J Chem Technol Biotechnol.*, **93**, pp. 2602–2616 (2018). https://doi.org/10.1002/jctb.5614.

27. Ghadimi, A., Mohammadi, T., and Kasiri, N. "Gas permeation, sorption and diffusion through PEBA/$SiO_2$ nanocomposite membranes (chemical surface modification of nanopar ticles)", *Int J Hydrogen Energy*, **40**, pp. 9723–9732 (2015). https://doi.org/10.1016/j.ijhydene.2015.06.013.

28. Ghadimi, A., Mohammadi, T., and Kasiri, N. "A novel chemical surface modification for the fabrication of PEBA/$SiO_2$ nanocomposite membranes to separate $CO_2$ from syngas and natural gas streams", *Ind. En. Chem. Res.*, **53**, pp. 17476–17486 (2014). https://doi.org/10.1021/ie503216p.

29. Mahdavi, H.R., Azizi, N., and Mohammadi, T. "Performance evaluation of a synthesized and characterized Pebax1657/PEG1000/$\gamma$-$Al_2O_3$ membrane for $CO_2/CH_4$ separation using response surface methodology", *J. Polym. Res.*, **24**(67) (2017). https://doi.org/10.1007/s10965-017-1228-1.

30. Chung, T.S., Jiang, L.Y., Li, Y., et al. "Mixed Matrix Membranes (MMMs) comprising organic polymers with dispersed inorganic fillers for gas separation", *Prog. Polym. Sci.*, **32**, pp. 483–507 (2007). https://doi.org/10.1016/J.PROGPOLYMSCI.2007.01.008.

31. Amini, Z. and Asghari, M. "Preparation and characterization of ultra-thin poly ether block amide/nanoclay nanocomposite membrane for gas separation", *Appl. Clay Sci.*, **166**, pp. 230–241 (2018). https://doi.org/10.1016/j.clay.2018.09.025.

32. Zhuang, G.L., Wey, M.Y., and Tseng, H.H. "The density and crystallinity properties of PPO-silica mixed-matrix membranes produced via the in situ sol-gel method for $H_2/CO_2$ separation. II: Effect of thermal annealing treatment", *Chem Eng Res Des*, **104**, pp. 319–32 (2015).

33. Laghaei, M., Sadeghi, M., Ghalei, B., et al. "The role of compatibility between polymeric matrix and silane coupling agents on the performance of mixed matrix membranes: polyethersulfone/MCM-41", *J. Membr. Sci.*, **513**, pp. 20–32 (2016).

34. Kojabad, M.E., Babaluo, A., Tavakoli, A., et al. "Comparison of acidic and basic ionic liquids effects on dispersion of alumina particles in Pebax composite membranes for $CO_2/N_2$ separation: Experimental Study and molecular simulation", *J. Environ. Chemical. Engin.*, **9**, 118494 (2021). https://doi.org/10.1016/j.seppur.2021.118494.

35. Kayser, M.J., Reinholdt, M.X., and Kaliaguine, S. "Amine grafted silica/SPEEK nanocomposites as proton exchange membranes", *J. Phys. Chem.*, B, **114**, pp. 8387–95 (2010).

36. Shamsabadi, A.A., Seidi, F., Salehi, E., et al. "Efficient $CO_2$-removal using novel mixed-matrix membranes with modified $TiO_2$ nanoparticles", *J. Mater. Chem.A*, **5**, pp. 4011–4025 (2017). https://doi.org/10.1039/C6TA09990D.

37. Prashanth, P.A., Raveendra, R.S., Krishna, R.H., et al. "Synthesis, characterizations, antibacterial and photoluminescence studies of solution combustion-derived $\alpha$-$Al_2O_3$ nanoparticles", *J. Asian Ceram. Soc.*, **3**, pp. 345–351 (2015). https://doi.org/10.1016/j.jascer.2015.07.001.

38. Mozaffari, V., Sadeghi, M., Fakhar, A., et al. "Gas separation properties of polyurethane/poly(ether-block-amide) (PU/PEBA) blend membranes", *Sep. Purif. Technol.*, **185**, pp. 202–214 (2017). https://doi.org/10.1016/j.seppur.2017.05.028.

39. Liu, S.L., Shao, L., Chua, M.L., et al. "Recent progress in the design of advanced PEO-containing membranes

for $CO_2$ removal", *Prog. Polym. Sci.*, **38**, pp. 1089–1120 (2013). https://doi.org/10.1016/j.progpolymsci.2013.02.002.

40. Sanders, D.F., Smith, Z.P., Guo, R., et al. "Energy-efficient polymeric gas separation membranes for a sustainable future: A review", *Polym.*, **54**, pp. 4729–4761 (2013). https://doi.org/10.1016/j.polymer.2013.05.075.
41. Lin, H., He, Z., Sun, Z., et al. "$CO_2$ selective membranes for hydrogen production and $CO_2$ capture - Part I: Membrane development", *J. Membr. Sci.*, **457**, pp. 149–161 (2014). https://doi.org/10.1016/j.memsci.2014.01.020.
42. Sadrzadeh, M., Amirilargani, M., Shahidi, K., et al. "Gas permeation through a synthesized composite PDMS/PES membrane", *J. Membr. Sci.*, **342**, pp. 236–250 (2009). https://doi.org/10.1016/j.memsci.2009.06.047.
43. George, G., Bhoria, N., Alhallaq, S., et al. "Polymer membranes for acid gas removal from natural gas", *Sep. Purif. Technol.*, **158**, pp. 333–356 (2016). https://doi.org/10.1016/j.seppur.2015.12.033.
44. Li, Y., Li, X., Wu, H., et al. "Anionic surfactant-doped Pebax membrane with optimal free volume characteristics for efficient $CO_2$ separation", *J. Membr. Sci.*, **49**, pp. 460–469 (2015). https://doi.org/10.1016/J.MEMSCI.2015.06.046.
45. Liu, Y., Chen, C., Lin, G., et al. "Characterization and molecular simulation of Pebax-1657 based mixed matrix membranes incorporating $MoS_2$ nanosheets for carbon dioxide capture enhancement", *J. Membr. Sci.*, **582**, pp. 358–366 (2019). https://doi.org/10.1016/j.memsci.2019.04.025.
46. Jeyranpour, F., Alahyarizadeh, G., and Minuchehr, A. "The thermo-mechanical properties estimation of fullerene-reinforced resin epoxy composites by molecular dynamics simulation - A comparative study", *Polym.*, **88**, pp. 9–18 (2016). https://doi.org/10.1016/J.POLYMER.2016.02.018.
47. Golzar, K., Modarress, H., and Amjad-iranagh, S. "Separation of gases by using pristine , composite and nanocomposite polymeric membranes: A molecular dynamics simulation study", *J. Membr. Sci*, **539**, pp. 238–256 (2017). https://doi.org/10.1016/j.memsci.2017.06.010.
48. Tocci, E., Gugliuzza, A., DeLorenzo, L., et al. "Transport properties of a co-poly(amide-12-b-ethylene oxide) membrane: A comparative study between experimental and molecular modelling results", *J. Membr. Sci.*, **323**, pp. 316–327 (2008). https://doi.org/10.1016/j.memsci.2008.06.031.

## Biographies

**Mahdi Elyasi Kojabad** has a PhD degree in Chemical Engineering and has spent all his three university courses at Sahand University of Technology. His interests include writing, original draft preparation, conceptualization, software, and investigation.

**Mahdi Nouri** is a MSc student of Chemical Engineering that graduated from Sahand University of Technology. He has contributed to this work with molecular simulation.

**Ali Akbar Babaluo** is a Full Professor at Sahand University of Technology and graduated from Tarbiat Modares University. In this article, he has contributed to this work with project administration, resources, writing including review and editing, and supervision.

**Akram Tavakoli** is an Associate Professor at Sahand University of Technology who graduated from Amir Kabir University and contributed to writing including review and editing as well as supervision.

**Rahim Sardari** is a MSc student of Chemical Engineering that graduated from Sahand University of Technology. He has helped with the investigation part of this article.

**Zeinab Farhadi** is a MSc student of Chemical Engineering that graduated from Sharif University of Technology. She has helped with writing including review and editing part of this article.

**Mahmoud Moharrami** is a MSc student of Chemical Engineering that graduated from Sahand University of Technology. He has helped with writing including review and editing part of this article.